Chemical Physics Letters 635 (2015) 157–162

Contents lists available at ScienceDirect

Chemical Physics Letters

journal homepage: www.elsevier.com/locate/cplett

Effects of inherent *rf* field inhomogeneity on heteronuclear decoupling in solid-state NMR

Rudra N. Purusottam[a,b,c], Geoffrey Bodenhausen[a,b,c], Piotr Tekely[a,b,c,*]

[a] *École Normale Supérieure – PSL Research University, Paris, France*
[b] *Sorbonne Universités, UPMC University, Paris 06, Paris, France*
[c] *CNRS, UMR 7203 LBM, Paris, France*

ARTICLE INFO

Article history:
Received 4 May 2015
In final form 17 June 2015
Available online 29 June 2015

ABSTRACT

Efficient heteronuclear decoupling is essential to obtain high-resolution NMR spectra of organic and biological solids containing protons and low-gamma nuclei such as carbon-13. All modern decoupling sequences employ pulse lengths that are optimized for a given radio-frequency (*rf*) power. However, there is an unavoidable distribution of *rf* field amplitudes across the volume of the sample. Inevitably, the effect of the *rf* field distribution manifests itself for fully packed rotors during any decoupling irradiation. In this study we present a detailed analysis of the effect of the inherent *rf* field inhomogeneity on decoupling by the low-power phase-inverted supercycled sequence for attenuation of rotary resonance (PISSARRO). This reveals a potential for further improvements of its efficiency.

1. Introduction

Heteronuclear decoupling is of prime importance to obtain high-resolution NMR spectra of organic and biological solids containing protons and dilute nuclei such as carbon-13. In polycrystalline or amorphous powders studied using fast magic-angle spinning (MAS), where flip-flop exchange between abundant protons is not very efficient, the performance of continuous-wave (CW) decoupling is poor [1]. Similar situations occur at moderate spinning frequencies in partially deuterated samples and in soft solids. This drawback has been overcome in the mid-1990s by replacing CW radio-frequency (*rf*) irradiation by phase-alternated pulses [1], which offer substantial improvement in decoupling efficiency at high spinning frequencies. This was followed by the popular two-pulse phase-modulated (TPPM) technique [2] and its variants [3–7], as well as a number of more recent decoupling schemes [8–11]. All modern decoupling sequences use pulse lengths that must be optimized for a given *rf* power. However, there exists an inherent distribution of *rf* field amplitudes, mostly along the axis of the solenoidal coil. Typically, the relative *rf* amplitude varies from 1.0 in the center of the coil to about 0.5 at its edges. To the best of our knowledge, the consequences of the *rf* inhomogeneity on the performance of heteronuclear decoupling have not been thoroughly examined so far. Very recently, we have demonstrated by numerical simulations, both in high- and low-power decoupling regimes, that the loss of the peak height due to the inhomogeneity of the *rf* field can reach as much as 40% for a sample with a length equal to that of the solenoidal coil [12]. Here we present a detailed analysis of the effects of the *rf* field inhomogeneity on the low-power phase-inverted supercycled sequence for attenuation of rotary resonance (PISSARRO) [8]. Similar effects are expected in the high-power regime and for other decoupling schemes. We discuss alternative ways for improving the efficiency of PISSARRO decoupling by minimizing the impact of the inherent *rf* field inhomogeneity along the axis of the solenoidal coil.

1.1. Experiments, materials and numerical simulations

All experiments were run on 400 and 850 MHz spectrometers with 1.3 mm rotors spinning at a frequency $\nu_{rot} = 60$ kHz. Uniformly ^{13}C, ^{15}N labeled L-histidine was purchased from Cambridge Isotopes and used without further purification. For spatially restricted samples, the top and bottom parts of the rotor were filled with compressed KBr powder. Other experimental details are included in the figure captions. All numerical simulations were carried out with SPINEVOLUTION [13], considering the 5-spin system $C^{\alpha}H^{\alpha}H^{\beta 1}H^{\beta 2}H^{N}$ of L-histidine hydrochloride monohydrate, with internuclear distances derived from the crystallographic structure.

* Corresponding author.
E-mail address: Piotr.Tekely@ens.fr (P. Tekely).

http://dx.doi.org/10.1016/j.cplett.2015.06.051
0009-2614/

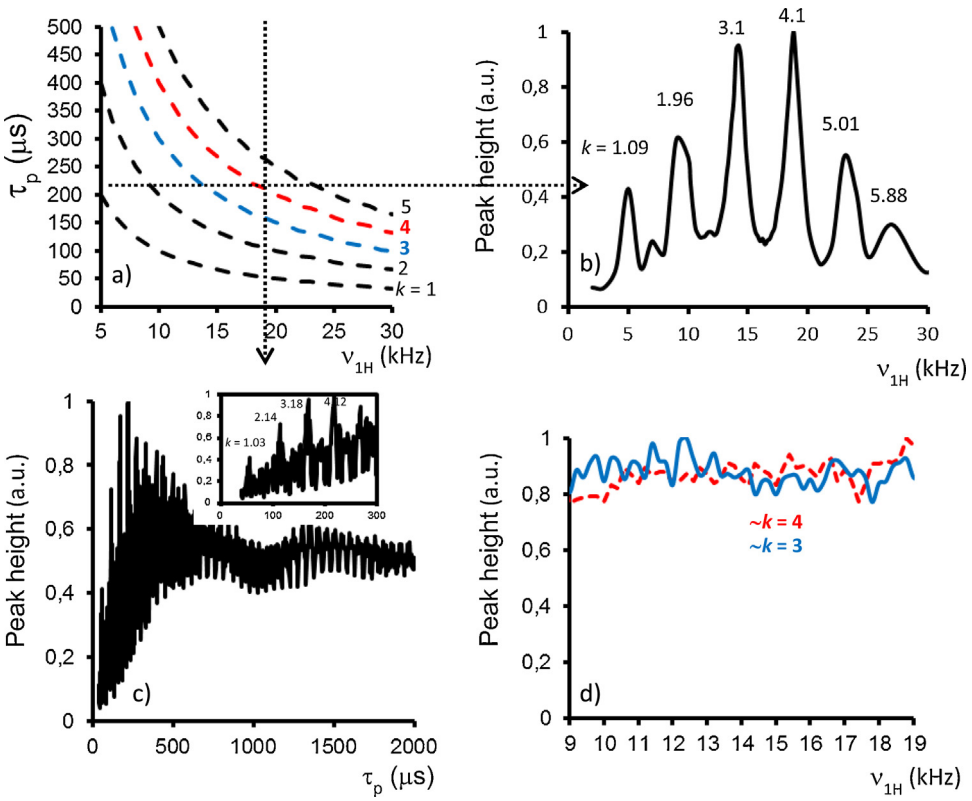

Figure 1. Numerical simulations of the efficiency of low-power PISSARRO decoupling in a magnetic field of 19.97 T (850 MHz for protons) for a spinning frequency of 60 kHz, assuming a perfectly homogeneous *rf* field. (a) Relationship between the pulse length τ_p and the *rf* amplitude ν_{1H} when the nutation angles β of the pulses are multiples of 2π, i.e., $\beta = 2\pi k$ where k is in the vicinity of integer values $k = 1, 2, \ldots$ (b) Numerical simulations of the height of the $^{13}C^{\alpha}H$ resonance of L-histidine as a function of the *rf* amplitude for a fixed pulse length $\tau_p = 218.16$ μs. (c) Simulated height of the $^{13}C^{\alpha}H$ resonance of L-histidine as a function of the pulse length for a fixed *rf* amplitude $\nu_{1H} = 18.8$ kHz. (d) Simulated height of the $^{13}C^{\alpha}H$ resonance of L-histidine as a function of the *rf* amplitude for optimized pulse lengths τ_p with nutation angles $\beta = 2\pi k$ in the vicinity of $k = 3$ and 4.

2. Results and discussion

2.1. Low-power PISSARRO decoupling with an ideal homogeneous rf field

Spinning at frequencies above 30 kHz may lead to a dramatic breakdown of the decoupling efficiency over a wide range of *rf* amplitudes. This is due to the phenomenon of rotary resonance recoupling (R^3), which can occur when the *rf* amplitude matches a multiple of the spinning frequency ($\nu_{1H} = n\nu_{rot}$) [14]. To overcome this drawback, PISSARRO decoupling was developed and shown to be effective in quenching rotary resonance recoupling in the vicinity of $n = 2$ [8]. The method also turned out to be very efficient at high *rf* amplitudes when $\nu_{1H} \gg \nu_{rot}$, far above any R^3 condition, as well as in a regime with low *rf* power and fast spinning, e.g., when $\nu_{1H} < \nu_{rot}$ [15]. This is due in part to its capacity to reduce interference between the modulation of dipolar couplings by the *rf* field and by spinning [8]. A thorough analysis of the mechanism of quenching of rotary resonance recoupling effects by the PISSARRO scheme has revealed the crucial role of mirror symmetry segments combined with phase shifts [16]. The immunity of PISSARRO decoupling against the offsets of remote protons, their chemical shift anisotropies and second-order cross-terms between these anisotropies and dipolar couplings has also been demonstrated [16,17].

To visualize the basic response of spin systems to low-power PISSARRO irradiation, Figure 1 shows simulations of the dependence of the decoupling efficiency as a function of the *rf* amplitude ν_{1H} (Figure 1b) and the pulse length τ_p (Figure 1c), assuming a perfectly homogeneous *rf* field and a static field of 19.97 T (850 MHz for protons) for a spinning frequency $\nu_{rot} = 60$ kHz. The relaxation induced homogeneous broadening and the inhomogeneous broadening of the resonance peaks was not included in the simulations. The figure shows that decoupling is most efficient when the pulse length τ_p is chosen so that the nutation angle β is in the vicinity of a multiple of 2π, i.e. $\beta = 2\pi\nu_{1H}\tau_p = k2\pi$ with integer $k = 1, 2, 3, \ldots$ According to our earlier observations, the undesirable 'dips' in Figure 1c are due to recoupling effects that occur when the pulse duration coincides with a multiple of a quarter the rotor period [8,14]. Note that the two highest maxima near $k = 3$ and 4 indicate a good performance over a wide range of *rf* amplitudes $10 < \nu_{1H} < 20$ kHz (Figure 1d). Analogous numerical simulations (not shown) for a static field $B_0 = 9.4$ T (400 MHz for protons) show a very similar response. This corroborates earlier observations of the effective immunity of PISSARRO against offsets of remote protons and their chemical shift anisotropies [15,16].

2.2. Effects of the inherent rf field inhomogeneity

As mentioned above, all modern decoupling sequences make use of pulse lengths that must be experimentally optimized for a given *rf* power. Naturally, there exists an inherent distribution of *rf* field amplitudes across the volume of a sample in a solenoidal coil. The effects may be appreciated in Figure 2 which shows nutation envelopes recorded for three differently packed rotors: (a) a fully packed rotor, (b) a sample with an axial length equal to and roughly coinciding with that of the solenoidal coil, and (c) a sample consisting of a ca. 1 mm disk that is located near the center of the coil. The top and bottom parts of the rotor were filled with compressed KBr powder. The striking differences in signal decay

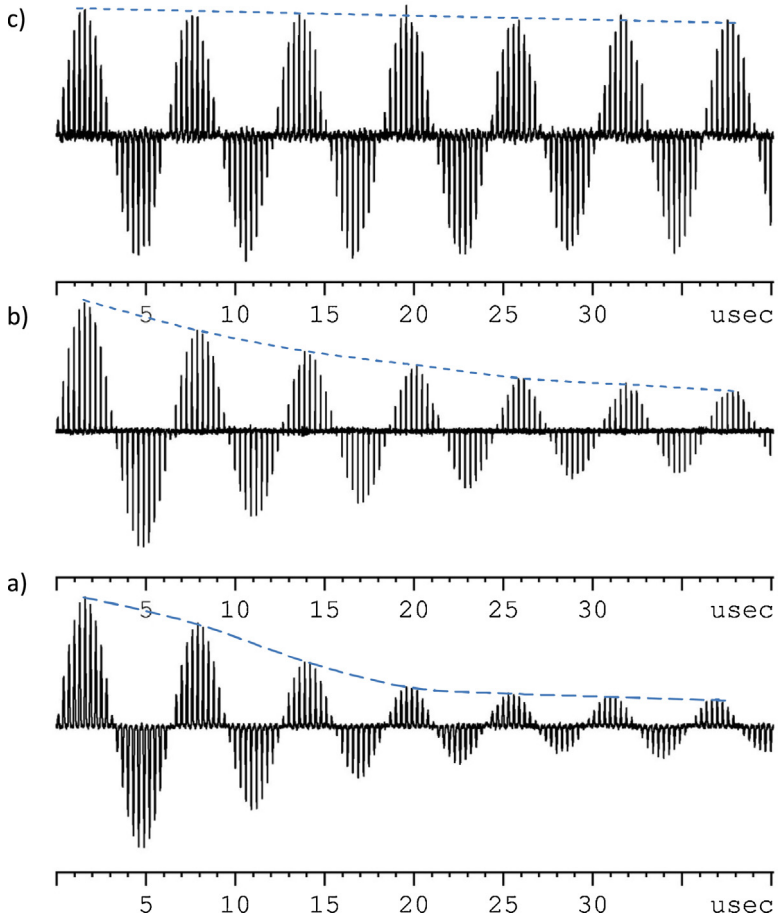

Figure 2. Experimental height of the $^{13}C^{\alpha}H$ peak of L-histidine as a function of the length of a ^{1}H pulse preceding cross-polarization, recorded for (a) a fully packed rotor, (b) a sample with an axial length roughly coinciding with the 2.5 mm length of the solenoidal coil, and (c) a sample with a thickness limited to ~1.0 mm (c). For (b) and (c) the top and bottom parts of the rotor (~1.25 mm and ~2.0 mm on both ends, respectively) were filled with plugs of KBr powder. All experiments were run at 400 MHz. For convenience, the nutation envelopes were normalized to the same maximum height; their actual amplitudes drop by about 10% in (b) and 50% in (c).

reflect the distribution of the *rf* field amplitude ν_{1H} across the volume of the sample. The most pronounced decay is observed for a fully packed rotor, this is due to signals from the top and bottom parts of the sample that are located near and beyond the edges of the coil. The decay is somewhat less pronounced when the sample has a length matched with the coil. A disk-shaped sample is naturally exposed to a more limited distribution of *rf* field amplitudes, although the decay due to such a distribution is not completely

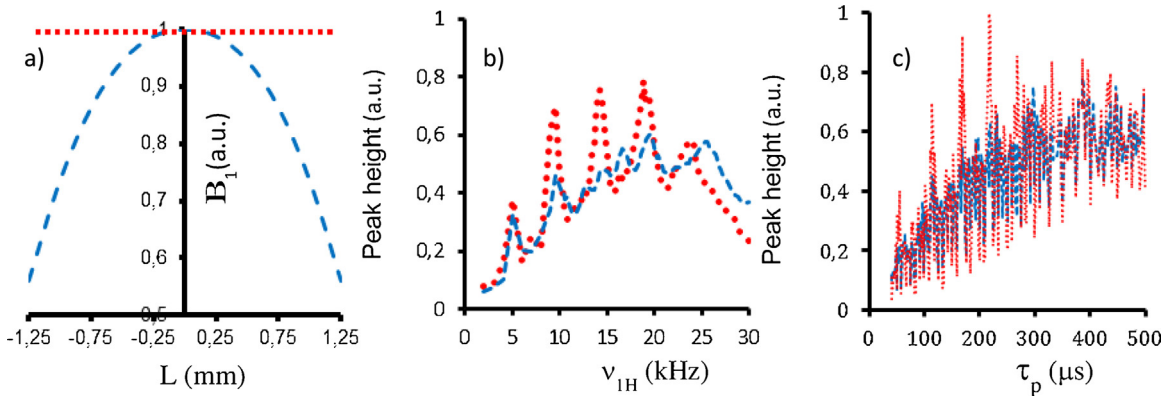

Figure 3. Effect of the inhomogeneity of the *rf* field on the efficiency of low-power PISSARRO decoupling. (a) The amplitude of the *rf* field B_1 calculated with the Biot–Savart law along the axis of a solenoidal coil with 1.5 mm internal diameter and 2.5 mm length (blue dashed line). The red dotted line refers to an ideal homogeneous *rf* field. (b) Calculated height of the $^{13}C^{\alpha}H$ resonance of L-histidine as a function of the nominal *rf* amplitude for a pulse length τ_p = 220 μs and an ideal homogeneous *rf* field (red dotted line) and for an inhomogeneous *rf* field (blue dashed line). (c) Calculated height of the $^{13}C^{\alpha}H$ resonance of L-histidine as a function of the pulse length τ_p for a nominal *rf* amplitude ν_{1H} = 18.8 kHz, either for an ideal homogeneous *rf* field (red dotted line) or for an inhomogeneous *rf* field (blue dashed line). The numerical simulations assumed a sample with a length equal to that of the solenoidal coil. All other parameters are as in Figure 1. (For interpretation of the references to color in this figure legend, the reader is referred to the web version of this article.)

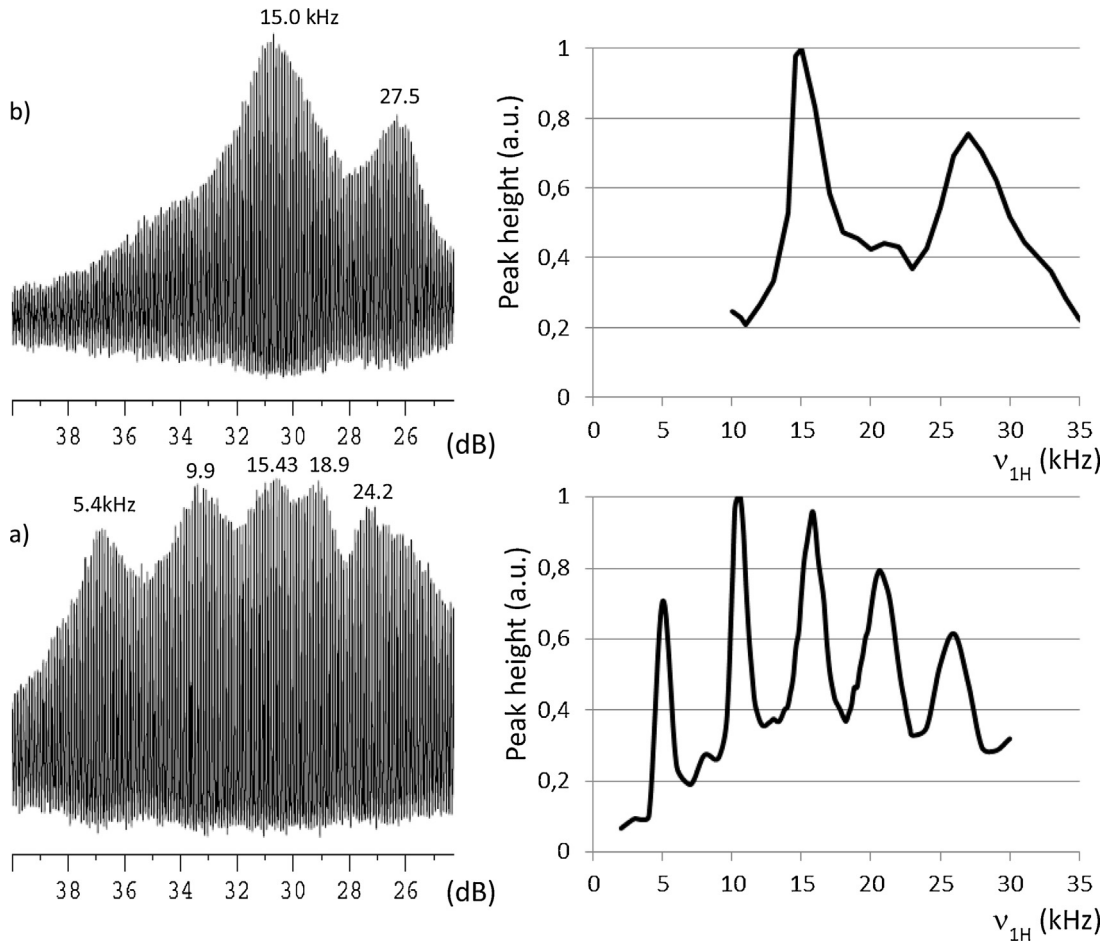

Figure 4. (Left) Experimental $^{13}C^{\alpha}H$ peak heights of a thin disk with a thickness of ~1.0 mm of L-histidine powder roughly centrally located with respect to the *rf* coil, recorded as a function of the decoupling *rf* amplitude, expressed in dB of attenuation. The top and bottom parts of the rotor were filled with KBr powder (two plugs of ~2.0 mm length). The spectra were obtained on a 400 MHz spectrometer with ν_{rot} = 60 kHz using a pulse length τ_p = 204 μs in (a) and τ_p = 69 μs in (b). (Right) corresponding $^{13}C^{\alpha}H$ peak heights calculated for the relevant *rf* inhomogeneities.

suppressed. Indeed, using phase-alternated pulses we checked that the remaining decay observed in Figure 1c is not due to relaxation effects.

To compare the decoupling performance in the presence and absence of *rf* inhomogeneities, one needs to know the actual variation of the *rf* field along the axis of a solenoidal coil. Figure 3a shows simulations of the *rf* field for a solenoidal coil with an inner diameter of 1.5 mm and a length of 2.5 mm, calculated using the Biot–Savart law. The relative *rf* intensity ranges from 1.0 in the center of the coil to 0.56 at its edges. To probe the consequences of this non-uniform *rf* field on the decoupling performance for a sample with a length equal to and coincident with the solenoidal coil, we have compared numerical simulations for an ideal homogeneous *rf* field. Since the main variation is along the axis of the solenoidal coil, we have omitted radial variations of the *rf* field near the edges of the solenoidal coil, although these may induce first-order spinning sidebands of small amplitude that is independent of the spinning frequency [18].

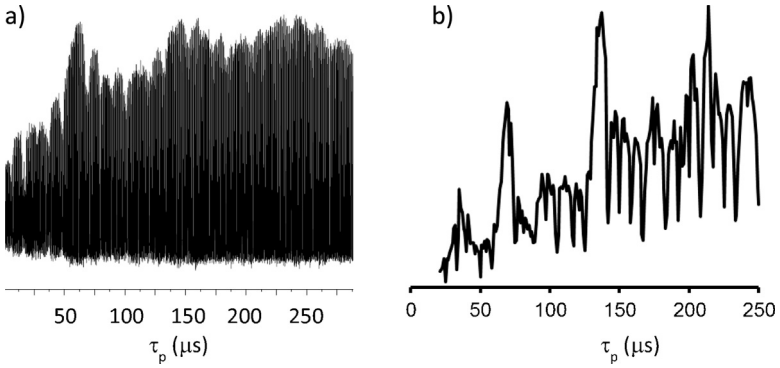

Figure 5. (a) Experimental $^{13}C^{\alpha}H$ peak heights of L-histidine as a function of the pulse length τ_p, recorded with an average *rf* decoupling amplitude $\langle\nu_{1H}\rangle$ = 14.8 kHz. The sample consisted of a thin disk of ~1.0 mm that was roughly centered with respect to the *rf* coil. The spectra were obtained at 400 MHz with a spinning frequency ν_{rot} = 60 kHz. (b) Calculated intensities of the $^{13}C^{\alpha}H$ peak with the same parameters.

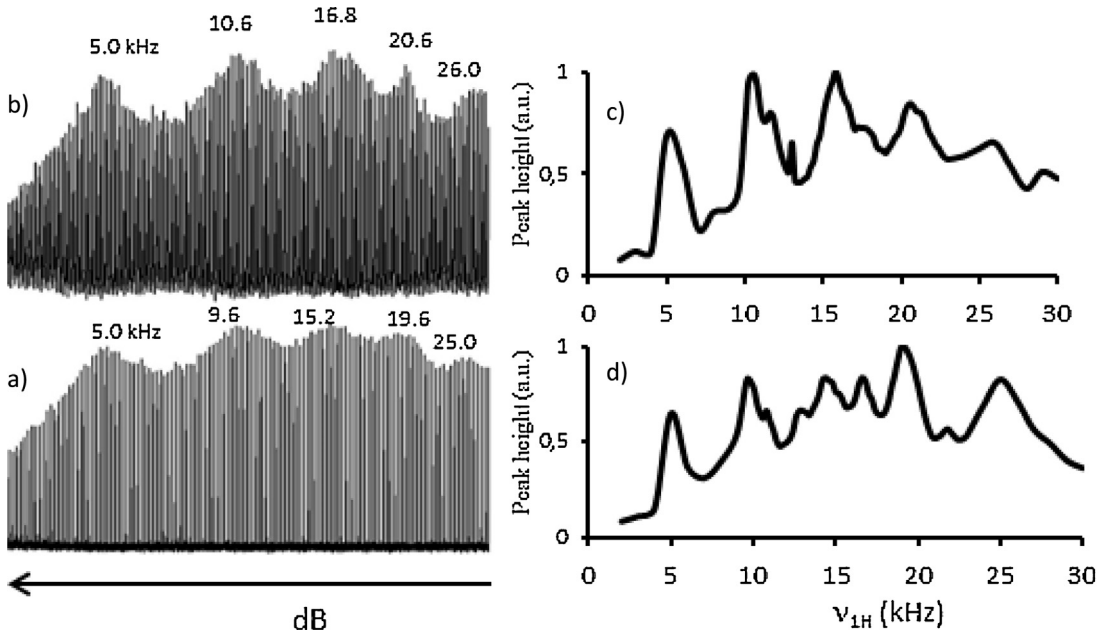

Figure 6. (Left) experimental $^{13}C^{\alpha}H$ peak heights of L-histidine recorded as a function of the decoupling *rf* amplitude. (a) For a sample having a length equal to that of the *rf* coil. (b) For a sample consisting of a disk of ~1.0 mm thickness that was roughly centered with respect to the *rf* coil. The spectra were obtained on a 400 MHz spectrometer with ν_{rot} = 60 kHz using optimized pulse lengths (a) τ_p = 218 μs and (b) τ_p = 202 μs for an average *rf* amplitude $\langle\nu_{1H}\rangle$ = 18.8 kHz. To facilitate the comparison, the experimental envelopes were normalized to the same maximum height; the actual drop in peak height is about 50% in (b). (Right) Corresponding envelopes of the $^{13}C^{\alpha}H$ peak heights calculated with the same parameters and relevant *rf* inhomogeneities.

As shown in Figure 3b and 3c, the *rf* field distribution leads to dramatic effects on the simulated peak heights. This is a direct consequence of different decoupling efficiencies at different locations in the sample for a given pulse length and nominal *rf* amplitude (vide infra). Figure 4 shows experimental intensities of $^{13}C^{\alpha}H$ peaks of a disk of L-histidine powder that is only ~1.0 mm thick and that is placed approximately in the center of the *rf* coil, recorded as a function of the *rf* amplitude. The intensities were calculated by assuming the same parameters with *rf* variations over 40% of the total coil length. The experimental maxima appear close to a nutation angle $\beta = 2\pi k$ with integer $k = 2, 3, \ldots$, a feature that is neatly reproduced by numerical simulations. However, despite the spatially restricted sample, the experimental intensities of the maxima are weaker, and they appear broader than in the calculated envelopes, especially for long pulse lengths τ_p. This is due to homogeneous and inhomogeneous broadening that was not included in the simulations, to the fact that the sample may not have been placed exactly in the center of the coil (vide infra), and that the slice of histidine powder may have been somewhat thicker than 1 mm. Similar differences are observed when comparing experimental and calculated intensities of the $^{13}C^{\alpha}H$ peaks as a function of the pulse length τ_p (Figure 5). As expected, the shorter the pulse lengths, the higher the *rf* amplitudes must be to reach the best decoupling efficiency with a nutation angle β close to a multiple of 2π (Figure 4).

Figure 6 shows experimental $^{13}C^{\alpha}H$ peaks of L-histidine as a function of the *rf* amplitude for a sample with a length equal to and roughly coinciding with that of the solenoidal coil, and for a slice of ca. 1 mm thickness positioned near the center of the coil. The heights of the $^{13}C^{\alpha}H$ peaks were calculated by averaging over the relevant *rf* distributions. For a sample that is exposed to a wide distribution of *rf* amplitudes, both the experimental and calculated envelopes have only hallow dips and are shifted in frequency for *rf* amplitudes below 20 kHz. To further probe the effects of the position of the sample, Figure 7 compares the envelopes of peak heights calculated for a slice of 1 mm thickness that is either centered with respect to the coil (blue solid line), or placed near the edge of the coil (green dotted line), compared with a sample having an axial length equal to and coinciding with that of the coil (red dashed line). Although the experimental envelope recorded for a centrally placed thin disk roughly reproduces the calculated envelope (blue solid line), its maxima are again strongly attenuated which must be mostly due to inhomogeneous broadening that is more pronounced in a high static field. Beside effects similar to those observed in Figures 4 and 6, a pronounced loss of peak height is calculated for low *rf* amplitudes when the disk is placed near the edge of the coil.

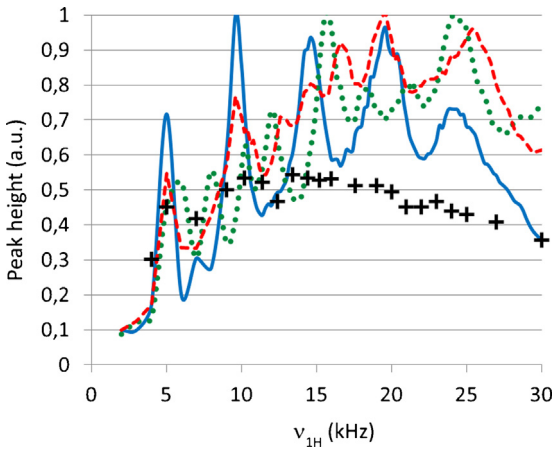

Figure 7. Calculated $^{13}C^{\alpha}H$ peak heights of L-histidine as a function of the nominal *rf* amplitude including the relevant inhomogeneity for a sample consisting of a thin disk of ~1.0 mm thickness that was assumed to be either (blue solid line) centered with respect to the *rf* coil or (green dotted line) placed near its edge. (Red dashed line): similar calculations for a sample having a length equal to that of the coil. All calculated graphs are normalized to the same maximum height. All numerical simulations used the same parameters. The experimental intensities (black crosses, arbitrary normalized) were recorded on a 850 MHz spectrometer with ν_{rot} = 60 kHz for a sample consisting of a thin slice of ~1.0 mm thickness that was roughly centered with respect to the *rf* coil, using a pulse length τ_p = 220 μs. (For interpretation of the references to color in this figure legend, the reader is referred to the web version of this article.)

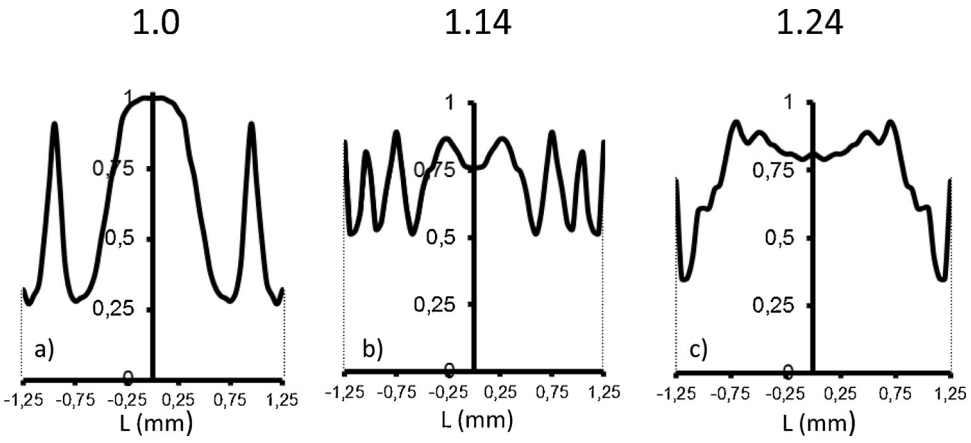

Figure 8. Spatial profiles of the $^{13}C^{\alpha}H$ peak heights calculated for pulse lengths (a) $\tau_p = 218$ μs, (b) $\tau_p = 386$ μs, and (c) using two different pulse lengths $\tau_p = 297$ and 386 μs in the basic phase-inverted pulse pair of the PISSARRO sequence, taking into account variations of the *rf* field along the axis of a coil of 2.5 mm length. All simulations assumed a nominal *rf* amplitude $\nu_{1H} = 18.8$ kHz, all other parameters being as in Figure 7. The numbers give the normalized integrated intensity (area under the graphs) of each spatial profile.

This is yet another indication that the *rf* field inhomogeneity plays a key role, since the efficiency of decoupling critically depends on the spatial position of the sample.

2.3. Toward a compensation for rf field inhomogeneity

Knowing the inherent variations of the *rf* field amplitude along the axis of a solenoidal coil and the response of the spin system to PISSARRO irradiation with a given pulse length and *rf* amplitude, one can visualize the idealized decoupling efficiency for different spatial positions of a sample having a length matched with the length of the coil (Figure 8). The spatial profile of the decoupling efficiency (as reflected in the peak height of the $^{13}C^{\alpha}H$ resonance of histidine) has been calculated for an optimal pulse length $\tau_p = 218$ μs and a nominal *rf* amplitude $\nu_{1H} = 18.8$ kHz (Figure 8a). As expected (see Figure 7), this reveals the best decoupling in the central part of the coil extending over 20% of its length, plus two narrow off-centered positions. However, the remaining spatial positions suffer from significant losses in decoupling efficiency that penalize the global performance. Remembering that PISSARRO decoupling with fully packed rotors is one of the most efficient [8,12,14,15] of all recently proposed schemes, losses due to the *rf* field distribution are expected to be similar for other decoupling pulse sequences. Although, as shown in Figure 8b, the dips in the peak heights of Figure 8a can be partially alleviated by using a longer pulse length $\tau_p = 386$ μs, this goes at the expense of the efficiency of decoupling in the central part of the coil. However, the integrated intensity (area under the graph) grows by 14% as compared with (a). Interestingly, an improved gain of 24% is predicted when combining two different pulse lengths within the phase-inverted basic pulse pair of the PISSARRO sequence (Figure 8c). This is due to the fact that the central part of the decoupling profile that comprises roughly 60% of the total coil length now appears more uniform. This suggests that the use of basic pulse pairs with two different pulse lengths could improve the global decoupling efficiency, especially in systems where homogeneous and inhomogeneous broadening of the resonance peaks is not too severe.

3. Conclusions

All modern decoupling sequences use pulse lengths that are optimized for a nominal *rf* amplitude. However, there is an inherent distribution of *rf* field amplitudes that has harmful effects for all decoupling schemes. We have demonstrated that for low power PISSARRO decoupling the distribution of the *rf* field across the volume of the sample can have a significant impact on the performance. Even for small samples, this can lead to a decrease of the peak heights. In spite of the fact that PISSARRO is one of the most efficient schemes, both in the high and low-power decoupling regimes, a detailed analysis has revealed further potential for improving its efficiency by employing variable pulse lengths to minimize the effects of the *rf* field inhomogeneity. This will be of special practical interest for systems with modest relaxation induced homogeneous broadening and conformation determined inhomogeneous broadening.

Acknowledgments

Financial support of the Ecole Doctorale ED 388 (UPMC University), the CNRS, the Ecole Normale Supérieure, the Fédération de Recherche (FR 3050) de l'Infrastructure de Recherche de Résonance Magnétique Nucléaire à Très Hauts Champs (IR RMN THC) of the CNRS is gratefully acknowledged.

References

[1] P. Tekely, P. Palmas, D. Canet, J. Magn. Reson. A 107 (1994) 129.
[2] A.E. Bennett, C.M. Rienstra, M. Auger, K.V. Lakshli, R.G. Griffin, J. Chem. Phys. 103 (1995) 6951.
[3] Z. Gan, R.R. Ernst, Solid State NMR 8 (1997) 153.
[4] B.M. Fung, A.K. Khitrin, K. Ermolaev, J. Magn. Reson. 142 (2000) 97.
[5] K. Takegoshi, J. Mizokami, T. Terao, Chem. Phys. Lett. 341 (2001) 540.
[6] R.S. Thakur, N.D. Kurur, P.K. Madhu, Chem. Phys. Lett. 426 (2006) 459.
[7] M. Kotecha, N.P. Wickramasinghe, Y. Ishii, Magn. Reson. Chem. 45 (2007) S221.
[8] M. Weingarth, P. Tekely, G. Bodenhausen, Chem. Phys. Lett. 466 (2008) 247.
[9] J.M. Vinther, A.B. Nielsen, M. Bjerring, E.R.H. van Eck, A.P.M. Kentgens, N. Khaneja, N.C. Nielsen, J. Chem. Phys. 137 (2012) 214202.
[10] V. Agarval, T. Tuherm, A. Reinhold, J. Past, A. Samoson, M. Ernst, B.H. Meier, Chem. Phys. Lett. 583 (2013) 1.
[11] A. Equbal, S. Paul, V.S. Mithu, J.M. Vinther, N.C. Nielsen, P.K. Madhu, J. Magn. Reson. 244 (2014) 68.
[12] R.N. Purusottam, G. Bodenhausen, P. Tekely, Chem. Phys. Lett. 614 (2014) 220.
[13] M. Veshtort, R.G. Griffin, J. Magn. Reson. 178 (2006) 248.
[14] T.G. Oas, R.G. Griffin, M.H. Levitt, J. Chem. Phys. 89 (1988) 692.
[15] M. Weingarth, G. Bodenhausen, P. Tekely, J. Magn. Reson. 199 (2009) 238.
[16] M. Weingarth, G. Bodenhausen, P. Tekely, Chem. Phys. Lett. 502 (2011) 259.
[17] M. Weingarth, J. Trébosc, J.P. Amoureux, G. Bodenhausen, P. Tekely, Solid State NMR 40 (2011) 21.
[18] P. Tekely, M. Goldman, J. Magn. Reson. 148 (2001) 135.